Conductance and kinetics of single cGMP-activated channels in salamander rod outer segments

W. Rowland Taylor* and Denis A. Baylor

Department of Neurobiology D-239, Fairchild Science Building, Stanford University School of Medicine, Stanford, CA 94305, USA

1. The conductance and kinetics of single 3′,5′-cyclic guanosine monophosphate (cGMP)-activated channels of retinal rod outer segments were studied in inside-out membrane patches. The size of the single channel currents was increased by using low concentrations of divalent cations.

2. At saturating cGMP concentration, the current flickered at high frequency. Occasionally, the current was interrupted by closures lasting tens or hundreds of milliseconds. At +50 mV the maximum current during an opening was slightly more than 1 pA, but the open channel level was poorly resolved due to the speed of the gating transitions.

3. Amplitude histograms confirmed the presence of a sublevel of current, roughly a quarter the size of the peak current, at low cGMP concentrations. The fraction of time in the sublevel decreased with increasing cGMP concentration, suggesting that the sublevel may be due to opening by the partially liganded channel.

4. Consistent with previous macroscopic current recordings, single channel activation by cGMP had an apparent dissociation constant of 8·6 μM, and a Hill coefficient of 2·8.

5. At saturating cGMP concentrations, the channel was modelled as a two-state system with the following parameters. The open channel conductance was 25 pS. The opening rate constant, β, was $1{\cdot}5 \times 10^4$ s^{-1} at 0 mV, and had a voltage sensitivity equivalent to the movement of 0·23 electronic charges outward through the membrane electric field. The closing rate constant, α, was $2{\cdot}1 \times 10^4$ s^{-1} and was voltage insensitive. Assuming that the open-state chord conductance was voltage independent, the inferred voltage dependence of β largely accounted for the outward rectification in the steady-state macroscopic current–voltage relation of multichannel patches, at saturating cGMP concentration.

Although the physiological role of the cGMP-gated channel in vertebrate photoreceptors has been known for some years (Fesenko, Kolesnikov & Lyubarsky, 1985; Haynes, Kay & Yau, 1986; Zimmerman & Baylor, 1986; Matthews, 1987), several basic questions about its function remain unresolved. For instance, the very rapid flicker in the current recorded from excised patches makes it difficult to resolve the open channel current. It has also been difficult to determine the rate constants for channel opening and closing in addition to the probability that the channel is open when fully liganded. Some of these problems are pointed out by Torre and his colleagues (Torre, Straforini, Sesti & Lamb, 1992; Sesti, Straforini, Lamb & Torre, 1994), who emphasize the unusual speed of the open–closed transitions.

The cGMP-activated channels from mammalian rod cells have been incorporated into planar lipid bilayers and expressed in frog oocytes (Hanke, Cook & Kaupp, 1988; Kaupp *et al.* 1989; Ildefonse & Bennett, 1991), but these channels appear to have different gating kinetics from those of excised patches from amphibian rod outer segments, which show much more rapid flicker. Some channels in inner segment patches from amphibia also flicker very little (Torre *et al.* 1992). Recently, a new subunit of the cGMP-activated channel of human rods has been discovered (Chen, Peng, Dhallan, Ahmed, Reed & Yau, 1993). When co-expressed with the subunit originally cloned from bovine rods (Kaupp *et al.* 1989), currents with very fast gating transitions, reminiscent of those in excised outer segment patches, were observed. More extensive

* Present address: Max-Planck-Institut für Hirnforschung, Neuroanatomische Abteilung, Deutschordenstrasse 46, D-60528 Frankfurt, Germany.

comparisons between the native and hetero-oligomeric channels may be required to determine how well the behaviour of the native channel has been replicated, and to gain an insight into the subunit composition of the native channel.

In an effort to find out more about the properties of the native channel, we recorded from outer segment patches that contained only a single channel. Although the search for these patches was arduous, several satisfactory recordings were obtained. Analyses of these recordings allowed us to make more refined estimates of several fundamental channel parameters.

METHODS

Preparation and recording

Inside-out patches were excised from rod outer segments obtained from larval tiger salamanders (*Ambystoma tigrinum*). Animals were killed by rapid decapitation and pithing. Under room light, outer segments were obtained by teasing apart pieces of isolated retina with fine needles. Retinae were isolated and stored in a solution containing (mM): NaCl, 110; KCl, 2; $CaCl_2$, 2; $MgCl_2$, 1; D-glucose, 10 and Na-Hepes, 5 (pH 7·45). After obtaining a seal and before excising the patch, the bathing solution was changed to a low divalent solution containing (mM): NaCl, 110; KCl, 2; EDTA, 0·1; Na-Hepes, 5 (pH 7·45). The patch pipettes were filled with this low divalent solution. Na-cGMP (Sigma, USA) was dissolved in distilled water to make a 100 mM stock solution and the concentration was verified in a spectrophotometer. A range of cGMP concentrations for the solutions bathing the patch was made by serial dilution. The chamber volume was approximately 0·2 ml. Solutions were perfused at 2–3 ml min^{-1}, and the chamber solution was completely exchanged within 30 s, as was evident from constant amplitude responses to cGMP in patches containing many channels.

Patch electrodes were made from fibre-filled borosilicate capillary tubing (1·2 mm o.d., 0·6 mm i.d., Glass Co. of America, Bargaintown, NJ, USA) and heavily coated with Sylgard® (elastomer no. 184; Dow Corning, Midland, MI, USA). Immediately before use, the tips were fire polished. Electrode resistances ranged from 4 to 7 MΩ. Spectral analysis of the electrode noise indicated that signals above about 8–10 kHz would be significantly attenuated (> −3 dB).

The patch pipette was connected to the amplifier by a Ag–AgCl wire which terminated about 1 cm from the electrode tip. Currents were recorded with an Axopatch 1B amplifier (Axon Instruments, Foster City, CA, USA). During single channel recording, voltage steps were usually limited to ±50 mV for no more than 10 s. Larger voltages often broke the patch but could be tolerated for shorter times. The recording electrode was withdrawn as far as possible from the chamber to minimize the immersed length. This helped minimize the input capacitance, thus reducing instrumental noise and improving the frequency response.

The patch current was low-pass filtered at 10 kHz and then sent to a PCM recorder (Neuro-Corder DR–484; Neuro Data Instruments Corp., New York) which digitized it at 44 kHz and recorded it on videotape. Subsequently, the recorded current was replayed through a 2·5 kHz low-pass filter and redigitized at 20 kHz. All filtering was done with an AI 2000 8-pole Bessel filter (Axon Instruments), and the cut-off frequencies (f_c) in this paper specify the −3 dB attenuation frequencies.

Recordings were made under visible light at a room temperature of 22–25 °C.

Analysis and simulations

As will be shown, channel gating was faster than the usable bandwidth of the recording system, and as a result it was not possible to measure the gating kinetics by conventional techniques such as threshold crossing analysis. As an alternative, we used a 'forward' approach. Model currents, generated by stochastic computer simulations with assumed parameters, were compared with experimental observations after similar filtering and analysis.

Current amplitude histograms, normalized to unit area (probability density functions; PDFs), were constructed from a minimum of 10 s of continuous recording, using a bin width of 0·015 pA; segments containing 'long gaps' (see below) were excluded. During construction of histograms, slight DC offsets in individual 0·2 s segments of the recorded current were removed by subtracting a baseline determined by eye. At saturating concentrations, 50 and 200 μM, the current rarely fell to baseline (zero current level) and DC offsets between individual segments were removed by adjusting the mean current during each segment to the same level.

At saturating concentrations of cGMP, the fully liganded channel was modelled as a two-state system, having one open-state and one closed-state. There are three parameters that define the model, the opening rate constant, β, the closing rate constant, α, and the amplitude of the events, î. The transition rate constants and open channel current were estimated by using computer simulations to construct theoretical PDFs from models of the channel activity. Exponentially distributed open and closed times were simulated by a pseudorandom number generator. Since the data acquisition board had a minimum output and sampling interval of 22 μs, simulations were performed at 1/11 real time. The measured impulse responses of the 8-pole Bessel low-pass filter at 250 and 2500 Hz were identical when the time axis was normalized. Simulated values for the current were output at an equivalent rate of 500 kHz and sampled at an equivalent rate of 20 kHz, after filtering at an equivalent rate of 2·53 kHz with the same Bessel filter used to process the experimental currents. The small difference in the equivalent filter cut-off was tolerated because the filter was only selectable to the nearest 10 Hz. The effects of additive instrumental noise were allowed for by convolving the simulated PDFs with a Gaussian density function having the same standard deviation as the current recorded in the absence of cGMP.

The simulation results were verified by fitting the probability density function:

$$f(y) = y^{a-1}(1-y)^{b-1}/B(a,b), \quad (1)$$

to the experimental PDFs (FitzHugh, 1983; Yellen, 1984), where $a = \alpha\tau$, $b = \beta\tau$ and $B(a,b)$ is the normalization factor. This equation, the beta distribution, describes the amplitude distribution of a two-state process filtered through a single-pole filter with a time constant, τ. Yellen (1984) calculated an empirical value that relates the −3dB cut-off frequency of a first-order filter to that of an 8-pole Bessel filter, and this value

was used to calculate τ; $\tau = 0{\cdot}228/f_{-3\,\mathrm{dB}}$. The effects of additive recording noise were allowed for by convolving the beta distributions with a Gaussian density function having the same standard deviation as the current recorded in the absence of cGMP. The beta distribution also provided a faster, more convenient method to perform the error analysis shown in Fig. 1.

Fitting models to data was completed by minimizing the function:

$$\chi^2 = \sum((I_i - I_{\mathrm{model}_i})/\sigma_i)^2, \quad (2)$$

where I_{model_i} is the predicted value and I_i is the measured value with standard deviation, σ_i. When fitting theoretical amplitude PDFs to the observed amplitude PDFs, we set $\sigma_i = 1$ for all i values, and we refer to this unweighted χ^2 value as D^2. The open channel amplitude, $\hat{\imath}$, was estimated from the PDF obtained at +50 mV. During fitting, $\hat{\imath}$ was held fixed and the rate constants varied to minimize D^2. This was repeated over a range of amplitudes to map out D^2 *versus* $\hat{\imath}$ as is shown for one patch in Fig. 8*A*. The final value of $\hat{\imath}$ was taken as that at the minimum of the parabola fitted to the D^2 points. The two rate constants were then recalculated using this new value for $\hat{\imath}$.

Calculations were performed to examine the precision of the rate-constant determination at a set amplitude. Figure 1*A* shows the optimal fit of the beta distribution to the +50 mV PDF from patch 1. The residuals plotted beneath the PDFs show that there was no systematic difference between the predicted and observed PDFs over the range 0·3–1·6 pA used for making the fit. The rate constants were varied between −15 and +15% of the optimal value, and the D^2 value was calculated. The circles in Fig. 1*B* show the result of varying the two rate constants individually. The sensitivities of the D^2 value to variations in either rate constant individually were similar. The open squares show the effect of varying the rate constants while maintaining the ratio β/α constant. The quality of the fit is less sensitive to concomitant changes in both rate constants that are positively correlated. The filled squares show the effect of an inverse or negative correlation between the rate constants, which produces a linear variation in the ratio β/α. The quality of the fit is comparatively much more sensitive to changes in the ratio between the rate constants. A 15% change in both α and β with fixed ratio produced the same change in D^2 as only a 3% change in both α and β with a variable ratio. Similar effects were seen at both positive and negative potentials.

The same value for $\hat{\imath}$ was assumed at both +50 and −50 mV, and therefore only the rate constants were fitted to the amplitude PDFs at −50 mV. This assumption is justified by the observations illustrated in Fig. 3*B*, which show that the instantaneous current–voltage relation of the channels was approximately linear between −50 and +50 mV.

The two rate constants were also estimated at saturating concentrations of cGMP by a 50% threshold analysis. This simply involved setting a threshold to 50% of the open channel amplitude, which was estimated by eye from the screen as 1·2 pA, and measuring times between threshold crossings. This same amplitude was used for all patches at both holding potentials. The exact time of threshold crossing was found from linear interpolation between the points that straddled the threshold. The rate constants derived from this type of

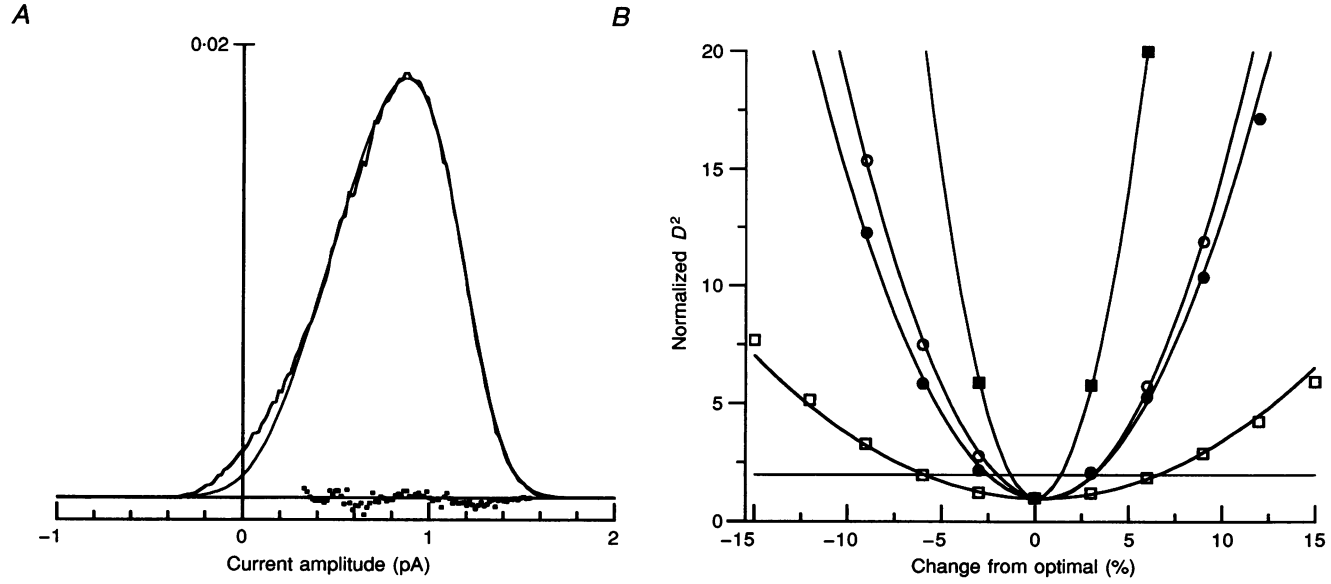

Figure 1. Fitting errors during analysis of amplitude PDFs

Patch 1, +50 mV, 200 μM cGMP. The ordinate scale for *A* is probability density per bin. *A*, the predicted beta distribution PDF, using the optimal values for β and α, is drawn through the data points. The difference between the predicted curve and the data, calculated over the range used for fitting, is shown by the points beneath the PDFs. *B*, D^2 is normalized to a minimum value of 1 and plotted against α (○) and β (●). The continuous horizontal line shows $D^2 = 2$. Initially the rate constants were simultaneously optimized for $\hat{\imath} = 1{\cdot}26$ pA, and then each in turn was varied between −15 and +15% of the optimal value. The curves show the best fitting quadratic functions. □, the effect of simultaneously changing β and α by the same percentage (positively correlated). ■, the effect of simultaneously changing β and α, by equal but opposite percentages (negatively correlated).

analysis proved to be sensitive to the selection of the threshold level, as Torre *et al.* (1992) have also noted, and therefore the accuracy of such results is questionable. Nevertheless, we have included results of threshold analyses to allow comparison of our results with those of previous workers.

RESULTS

Cyclic GMP-activated currents were recorded in excised inside-out patches, with divalent cations nominally absent from the solutions (none added, 0·1 mM EDTA). Thirty-five

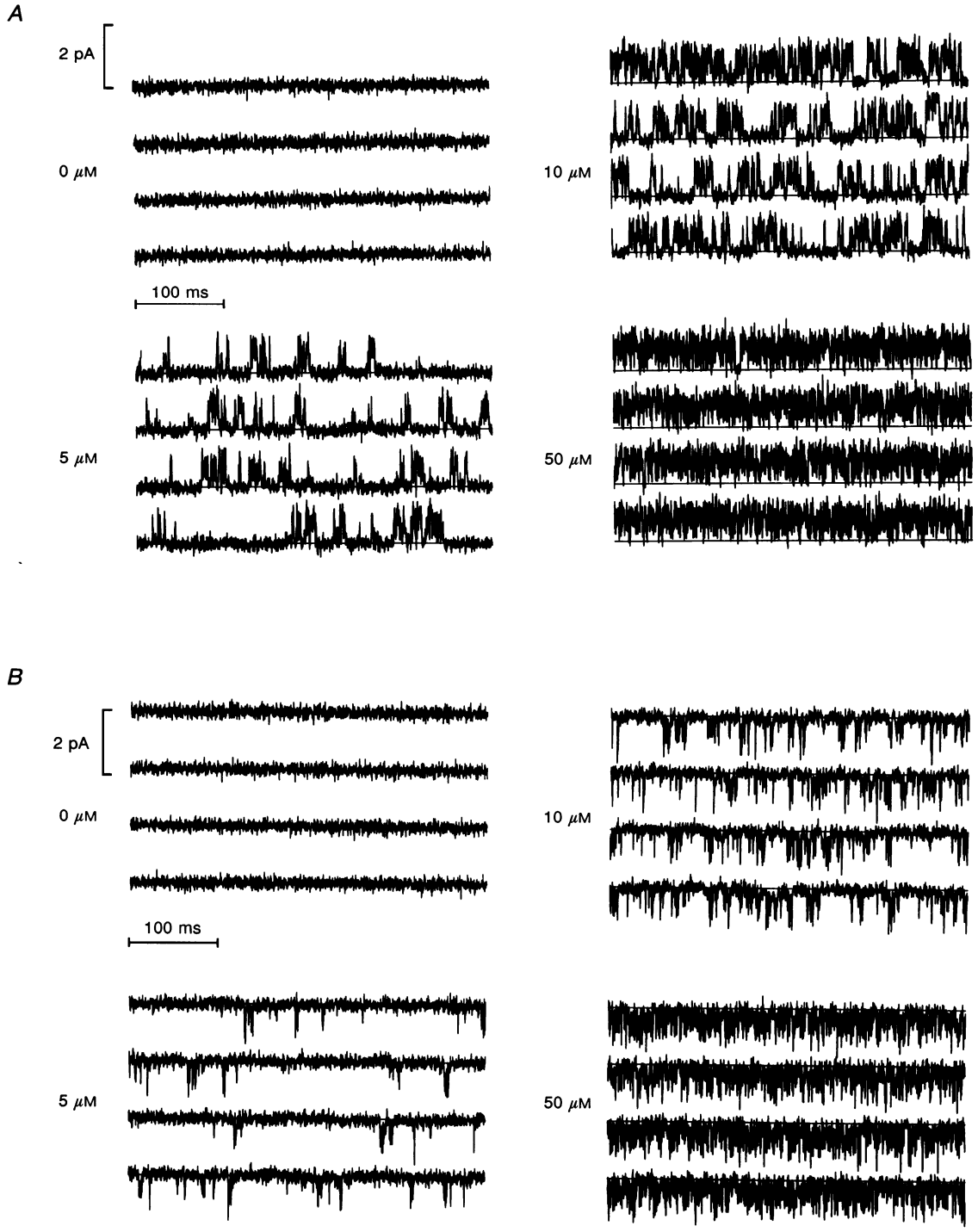

Figure 2. Single channel activity

Each panel shows a continuous recording at the indicated concentration of cGMP. In the absence of cGMP there was no channel activity. The continuous lines through the traces indicate the baseline or closed channel level. The patch was held at 0 mV and alternating 10 s voltage steps to ± 50 mV were applied every 15 s. The traces in *A* were recorded during steps to +50 mV, and those in *B* to −50 mV. Patch 3, filter f_c = 2500 Hz.

per cent of the patches tested gave a response to cGMP, and of these, 3 % contained only a single channel. Some patches initially failed to respond to cGMP because a vesicle formed upon excision, as evidenced by the appearance of a response to cGMP after the tip of the pipette was touched against a lump of silicone elastomer on the bottom of the chamber. Altogether nine patches containing a single channel were obtained, and of these, three gave recordings sufficiently stable and long lasting to be suitable for detailed analysis. Patches containing only a single channel could be identified unambiguously by the fact that the peak amplitude of the channel activity at +50 mV and saturating concentrations of cGMP was roughly 1 pA (see Fig. 2).

General characteristics of single channel activity

Figure 2 illustrates single channel activity in patch 3 at several concentrations of cGMP, with voltages of +50 (*A*) and −50 mV (*B*). In the absence of cGMP, no detectable

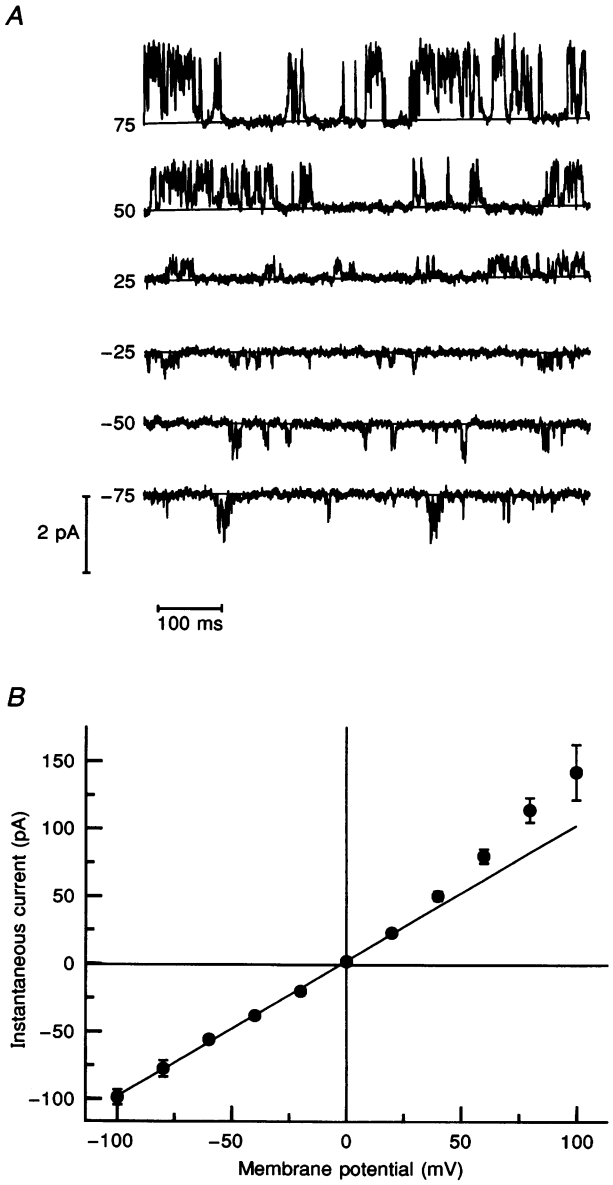

Figure 3. Current–voltage relation of the channel

A, single channel openings were observed at the membrane potentials (mV) indicated next to each trace in the presence of 5 μM cGMP. Filter $f_c = 1$ kHz, patch 1. No events were observed at 0 mV, the predicted reversal potential (trace not shown). *B*, the mean instantaneous current–voltage (I–V) relation measured from 4 cells (error bars show the standard deviation). Individual I–Vs were normalized to 1 nS conductance between −100 and +20 mV (mean conductance, 7·9 nS). Currents were activated by 200 μM cGMP. The net cGMP-gated current was obtained by subtracting patch current in the absence of cGMP from current in the presence of cGMP. Measurements were taken at a constant time point, either 20 or 40 μs after the time of the voltage step. The straight line was fitted to the I–V relation between −100 and +20 mV.

openings occurred and the current fluctuated at the baseline due to instrumental noise. In 5 μM cGMP many brief openings occurred. At both positive and negative voltages the openings occurred in bursts, which were separated by returns to the baseline (closed) level. At the highest concentrations of cGMP the bursts of openings were no longer discrete and instead fused into a continuous rapid flicker. Occasionally the flicker was interrupted by a closure that lasted long enough to hold the current at the baseline; one such closure is present in the first trace at 50 μM in Fig. 2*A*. At both +50 and −50 mV the current during openings reached a peak amplitude roughly 1 pA above the baseline, but the open channel current level was not well resolved, because the openings were brief compared with the settling time of the 2·5 kHz low-pass filter.

Comparison of panels *A* and *B* in Fig. 2 reveals that the channel activity was voltage dependent. At +50 mV the bursts of openings in 5 and 10 μM cGMP occurred more frequently than at −50 mV, and the mean current at 50 μM cGMP was larger. Figure 3*A* shows currents from patch 1 recorded in 5 μM cGMP over a wider range of voltages. The currents at +75 mV are larger than those at −75 mV, but because the open-state current was not well resolved, it is not clear whether this difference should be attributed to voltage dependence of the open channel conductance or to voltage dependence of the channel-gating kinetics. In an attempt to define the form of the open channel's instantaneous current–voltage relation, macroscopic currents from multichannel patches were measured at a fixed early time after a voltage step. The mean results from four patches, measured 20 or 40 μs after the onset of the voltage step are plotted in Fig. 3*B*. The form of the relation is virtually identical to that measured by Zimmerman & Baylor (1992) at 50 μs. Even though the relation was determined at an early time, at least part of the outward rectification in Fig. 3*B* should probably be attributed to the voltage dependence of very fast gating transitions in the channel (see below).

The channel activity induced by cGMP did not desensitize (Fesenko *et al.* 1985; Karpen, Zimmerman, Stryer & Baylor, 1988*b*). Even at the highest cGMP concentrations the channel openings were sustained at a constant average rate

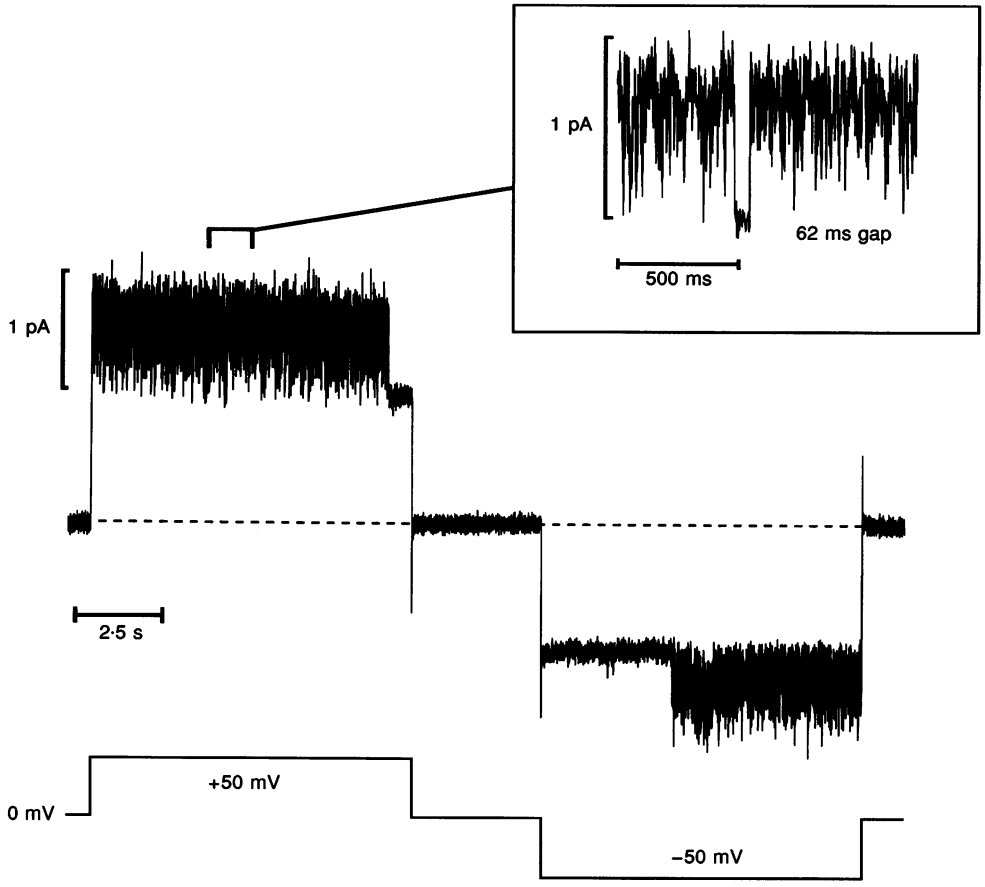

Figure 4. A long gap observed during the application of 200 μM cGMP

Patch 3. Channel activity ceased before the end of the step to +50 mV, and restarted after commencement of the step to −50 mV. It is possible that there were actually 2 long gaps since channel activity during the interval at 0 mV, the reversal potential, would not be detected. The inset shows, on a more expanded time scale, an example of a short gap that lasted 62 ms (see text).

for at least 10 s, the duration of the longest voltage step used. Occasionally, 'long gaps' (Matthews & Watanabe, 1988), lasting a fraction of a second to several seconds, occurred. One such event is illustrated in Fig. 4, which shows the current recorded during consecutive voltage steps to +50 and −50 mV. The channel became inactive before the end of the +50 mV step and reactivated after the start of the −50 mV step. The frequency of these events was roughly 9×10^{-3}, 13×10^{-3} and 17×10^{-3} long gaps per second, for patches 1, 2 and 3, respectively. The rarity of these events made it impossible to determine whether their frequency of occurrence depended on the concentration of cGMP.

The inset in Fig. 4 shows an example of another type of infrequent event which had a much shorter duration than

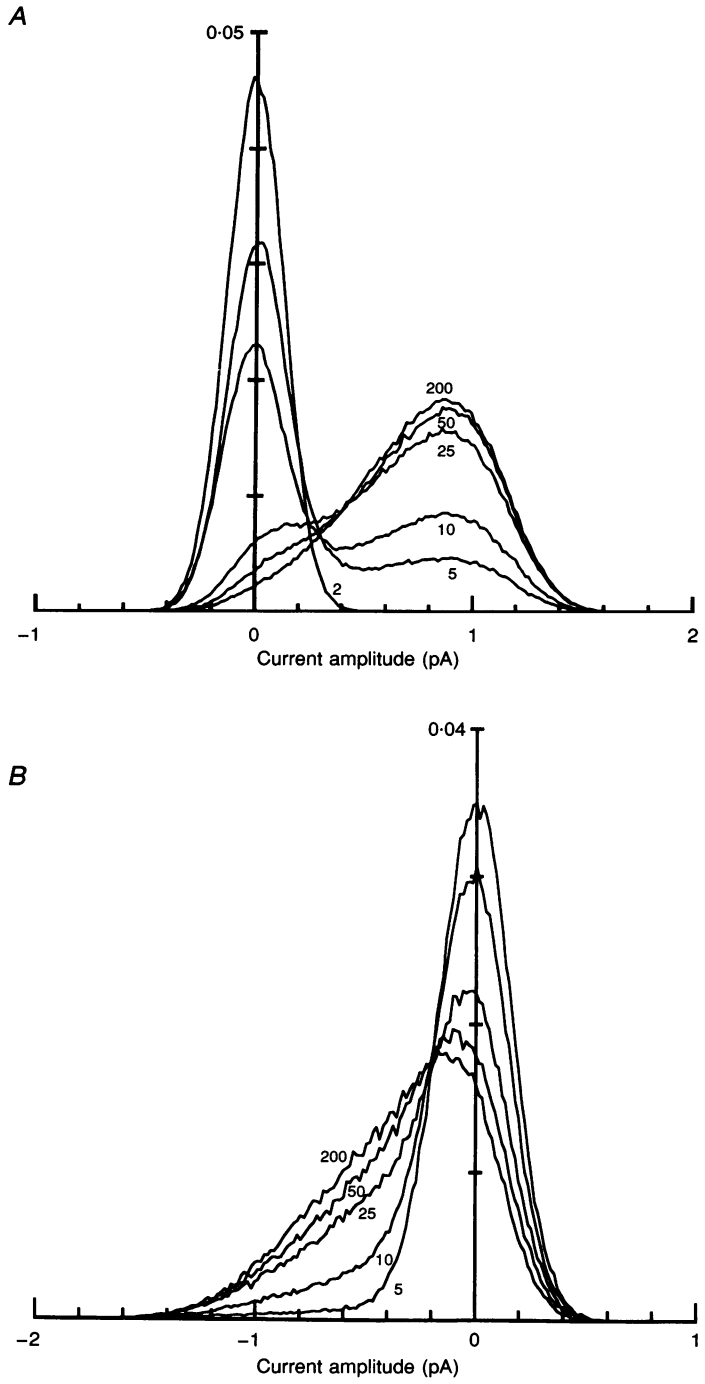

Figure 5. Amplitude PDFs constructed from continuous periods of channel activity

The ordinate scale is probability density per bin. Filter $f_c = 2500$ Hz. *A*, the concentrations of cGMP were 2, 5, 10, 25, 50 and 200 μM. Recorded at +50 mV, patch 1. *B*, the concentrations of cGMP were 5, 10, 25, 50 and 200 μM. Recorded at −50 mV, patch 3.

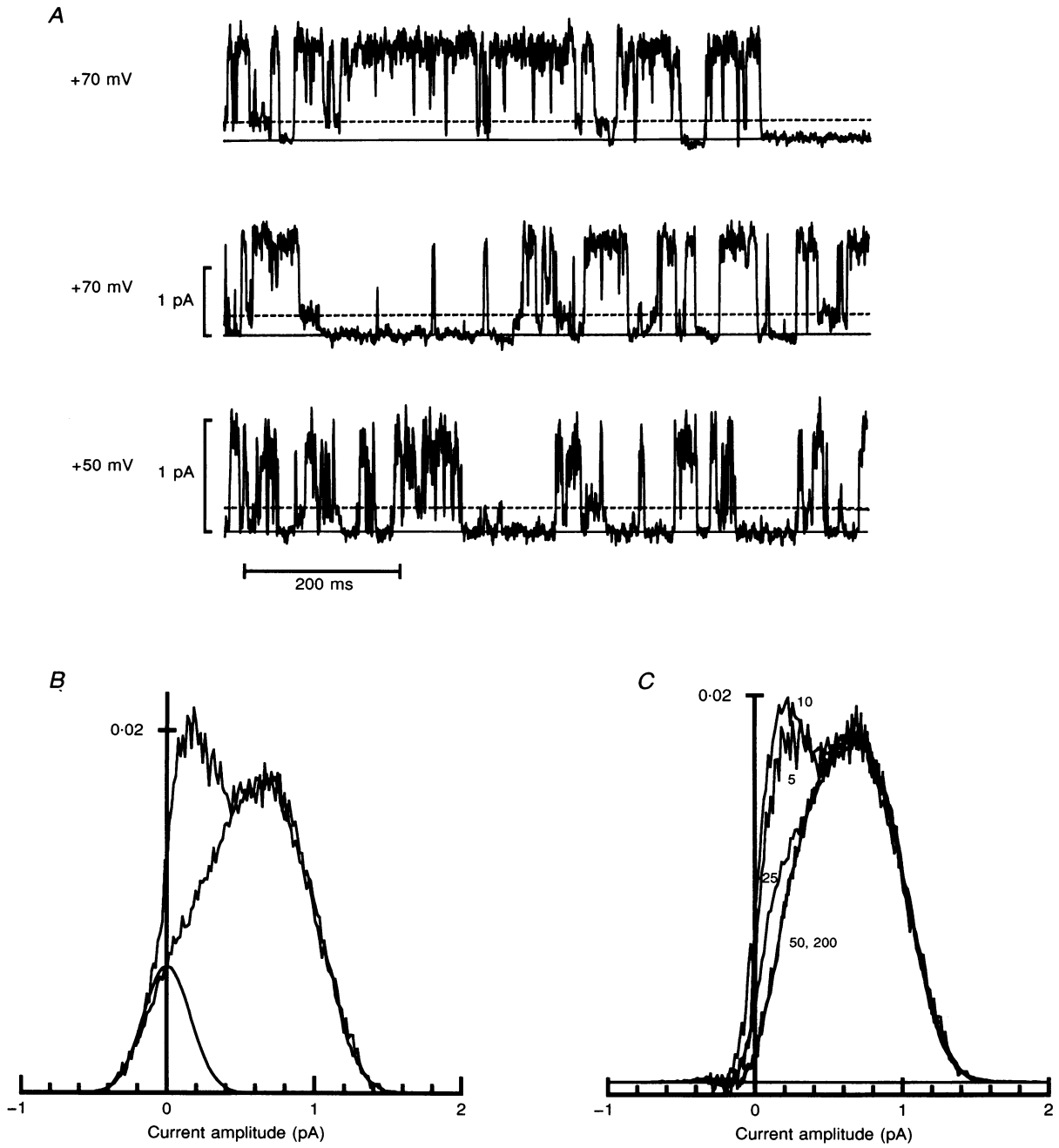

Figure 6. The small activated state of the channel

A, selected records showing channel activity in 5 μM cGMP at +70 (top 2 records) and +50 mV (bottom record). Patch 1, filter $f_c = 500$ Hz. Occupancy of the small activated state can be directly observed, and the approximate level is indicated by the dashed lines at 0·3 and 0·2 pA for +70 and +50 mV, respectively. The continuous line shows the closed level. *B*, patch 3, filter $f_c = 2500$ Hz. Superimposed amplitude PDFs in 5 and 200 μM cGMP. The 200 μM cGMP PDF has been arbitrarily scaled for comparison. The 5 μM cGMP PDF was obtained only from recorded segments containing obvious channel activity. This precluded distortion of the PDF due to subtraction of a very large baseline. The continuous line shows the residual baseline density that was subtracted to produce the 5 μM cGMP PDF shown in *C*. *C*, patch 3. Superimposed amplitude PDFs with the baseline components subtracted. Each has been scaled arbitrarily for comparison of the shapes. Note that the lobe at lower amplitudes, due to occupancy of the small activated state, gradually disappears as the concentration of cGMP is raised. The ordinate scale is probability density per bin for the 5 μM amplitude histogram.

that of the long gaps. A similar event is present in the top trace of the recordings in 50 μM cGMP in Fig. 2*A* and another in the recording in 50 μM cGMP in Fig. 2*B*, about 70 ms from the right end of the third trace down. These 'short gaps' may represent an additional closed-state of the channel.

Amplitude histograms constructed from recordings at +50 and −50 mV are illustrated in Fig. 5 as probability densities (PDFs). The ordinate is the fraction of the measured current amplitudes that fell within each 0·015 pA bin width. At +50 mV (Fig. 5*A*) two peaks can be seen. One represents the closed, quiescent state of the channel (amplitude 0 pA), and the other represents the state activated by cGMP, when the channel rapidly flickered open and closed. We shall define the closed, quiescent state of the channel as the 'inactive state', and that marked by rapid flicker as the 'activated state'. As expected, increasing concentrations of cGMP caused the relative area under the inactive state peak at 0 pA to decline and the area under the activated state peak to increase. The voltage dependence of channel activation by cGMP is evident when the PDFs at positive and negative voltage are compared: those at −50 mV (Fig. 5*B*) did not display an obvious second peak corresponding to the activated state, but instead became progressively more skewed toward negative amplitudes as the cGMP concentration was increased. We interpret this as indicating that hyperpolarization favours closed-states of the channel (see p. 578).

Inspection of the current amplitude distribution in Fig. 5*A* indicates that the conductance of an open channel cannot be immediately estimated from the separation between the baseline peak and the peak at saturating cGMP. The peak generated by channel activation was broader than the baseline peak. This implies that in the activated state the mean open time of the channel was short compared with the time constant of the recording system, and that the true open channel level must lie somewhere to the right of the peak in the PDF. An estimate of the current amplitude through the open channel is presented on p. 577.

Evidence for a sublevel dependence on cGMP concentration

Previous recordings from multichannel patches have suggested the existence of a subconductance state of the cGMP channel of rods (Haynes *et al.* 1986; Zimmerman & Baylor, 1986), and cones (Haynes & Yau, 1990), but such observations have not been reported by all authors (Matthews & Watanabe, 1988; Sesti *et al.* 1994). The records in Fig. 6*A*, obtained at +70 and +50 mV in 5 μM cGMP, show that the current often fluctuated near a sublevel about 0·25 pA above the baseline. We low-pass filtered these traces more severely ($f_c = 500$ Hz) than the records in Fig. 2, to resolve the substate level more clearly. The question arises, however, whether the small current represents an activated state with low open channel conductance or an activated state in which fast intrinsic gating transitions were heavily smoothed by the 500 Hz filter, to give a mean current near 0·25 pA. To examine this point, in addition to the concentration dependence of the small current level, amplitude PDFs obtained with a bandwidth of 2500 Hz (e.g. those in Fig. 5*A*) were analysed.

The PDFs in Fig. 5*A* do not show clear evidence for the 0·25 pA current level evident in Fig. 6*A*, but such small currents might be obscured by the humps representing the baseline noise and the activated state associated with large current. Therefore a Gaussian curve fitted to the baseline distribution (σ, 0·16 pA) was scaled and subtracted from the PDFs at each concentration. The resulting amplitude distributions from patch 3 are plotted in Fig. 6*C*. To minimize errors arising from subtraction of the relatively large baseline component for the 5 μM cGMP distributions, a different procedure was used. The records were viewed in sections, and, using manually controlled cursors, only segments containing clear channel activity were used to generate the amplitude distributions. The small residual baseline peak in the amplitude distributions was then removed by fitting a Gaussian curve to the left side of the amplitude distribution, as is shown for the 5 μM PDF in Fig. 6*B*.

For ease of comparison, the amplitude distributions in Fig. 6*C* have been scaled in order to superimpose the peaks resulting from the activated state of large amplitude. The distributions at 5 and 10 μM cGMP show an additional smaller peak centred near 0·2 pA, the level at which the dashed line is drawn in the lowest record of Fig. 6*A*. The plots in Fig. 6*C* indicate that the occurrence of the small currents depended on the cGMP concentration because the small peak became less prominent and eventually disappeared as the cGMP concentration rose. The simplest interpretation is that the small currents represent an activated state with lower peak conductance than the state occupied at saturating cGMP concentrations. An alternative possibility, which cannot be excluded, is that both activated states had the same open conductance, but unusually fast gating transitions, averaged by the low-pass filter, produced the small mean current of about 0·2 pA. Either notion implies that each activated state was associated with a characteristic open-state, and for simplicity, that associated with the smaller current level will be termed the 'small activated state'.

Dependence of channel activation on cGMP concentration

As described above, the baseline level of the PDFs was fitted well by a Gaussian curve with σ of 0·16 pA for a 2500 Hz bandwidth. Since the PDFs are normalized to unit area, the area under the baseline peak gives an estimate of the fraction of the time (P_{inactive}) that the channel was not in an activated state. Similarly, an estimate for the probability

that the channel was activated is $P_{active} = 1 - P_{inactive}$. These estimates would correspond to the respective probabilities that the channel was open and closed if the gating kinetics in the activated channel were well resolved. In our case, however, the recording system is relatively slow, and thus it is preferable to assign the peaks to activated and inactivated states.

We can divide P_{active} into two parts. The amplitude distributions in Fig. 6*C* suggest that there are two different activated states of the channel. The state associated with the smaller current is present some of the time at low cGMP concentrations, but at saturating cGMP concentrations (50 and 200 μM) it disappears and the state with the large current then dominates. If one assumes that at saturating cGMP the activated channel was always in the 'large activated state', the proportion of time spent in the smaller state, $P_{smallstate}$, at lower concentrations can be obtained by converting each amplitude distribution in Fig. 6*C* into a PDF and subtracting from each the area of the appropriately scaled 200 μM cGMP amplitude distribution, i.e:

$$P_{small\,state} = P_{active} - P_{large\,state}$$

and

$$P_{inactive} + P_{large\,state} + P_{small\,state} = 1.$$

The results are plotted in Fig. 7, which shows the dependence of the probability of each state on the cGMP concentration. With increasing cGMP, $P_{large\,state}$ (filled symbols) increased to a maximum of 0·94, while $P_{small\,state}$ (open symbols) passed through a maximum of 0·1 and then declined. These results are consistent with the notion that the channel is only partially liganded in the small activated state. The continuous line through the points shows the non-linear least-squares fit to the equation:

$$P = P_{max}\frac{[cGMP/K]^n}{1 + [cGMP/K]^n}, \quad (3)$$

where P is the probability that the channel is in the large activated state, $P_{max} = 0{\cdot}94$, the dissociation constant $K_d = 8{\cdot}6$ μM and the Hill coefficient $n = 2{\cdot}8$. This fit, which ignores the presence of the small activated state, is similar to the dose–response relation for the macroscopic current (Zimmerman & Baylor, 1986).

Transition rate constants and open channel conductance for the large state

The object of this section is to obtain estimates for the amplitude of the current through an open channel and for the rate constants that govern transitions between the open and closed-states, when the channel is in the large activated state. The small activated state was not analysed because the channel spent only short times in it, even at low concentrations of cGMP, and it was obscured by baseline noise and the fluctuations in the large state. When the channel was in the large state, the measured current trajectory fluctuated between the baseline and the true open channel level at frequencies that exceeded the usable recording bandwidth. This severely limited the usefulness of measurements of open and closed times as a method for obtaining kinetic parameters (but see Matthews & Watanabe, 1988; Haynes & Yau, 1990).

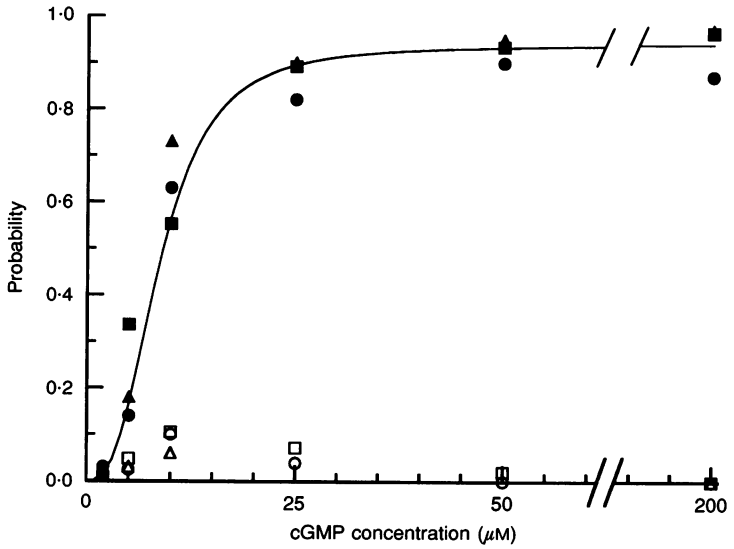

Figure 7. Probability measurements from amplitude PDFs

The filled symbols show the steady-state occupancy of the full conductance state, and the corresponding open symbols show the small activated state. Each symbol shows measurements from a different patch all at +50 mV. The continuous line was the fit to eqn (3) in the text, with $K_d = 8{\cdot}6$ μM and $n = 2{\cdot}8$.

In analysing the large activated state, we used records obtained in saturating cGMP, where the small state was negligible. We selected records that did not contain long gaps and we ignored short gaps by restricting the interval over which the fits were calculated. It was assumed that there were only two conductance states, closed and open. Using simulations (see Methods), we searched for three parameters that provided the best fit to the PDFs. These parameters were the opening rate constant (β), the closing rate constant (α) and the amplitude of the current through the open channel, $\hat{\imath}$. Figure 8*A* illustrates the determination of $\hat{\imath}$ for patch 3. The amplitude parameter was varied between 1·1 and 1·5 pA, and the normalized D^2 value (see Methods) for the best fit is plotted at each amplitude. The fit was restricted to the PDF amplitude range 0·3–1·5 pA (see below). The quadratic fit (Fig. 8*A*) to the results of the simulations has a minimum at 1·26 pA, corresponding to a chord conductance of 25·2 pS. Figure 8*B* illustrates the best fit to the amplitude PDF obtained from patch 3 at −50 mV and 200 μM cGMP. The simulation parameters were: $\beta = 0{\cdot}88 \times 10^4\ s^{-1}$, $\alpha = 2{\cdot}06 \times 10^4\ s^{-1}$, and $\hat{\imath} = -1{\cdot}26$ pA. The simulation fit to the amplitude PDF at +50 mV in Fig. 8*C* used the parameter values: $\beta = 2{\cdot}49 \times 10^4\ s^{-1}$, $\alpha = 2{\cdot}44 \times 10^4\ s^{-1}$ and $\hat{\imath} = 1{\cdot}26$ pA. The model provides a good fit to the experimental PDF, although there was a discrepancy at lower amplitudes which could not be accounted for by the two-state model. A similar trend was noted for all three patches. The excess experimental density at lower amplitudes is probably explained by the presence of short gaps.

The two-state model, with suitable parameters, provided a reasonable fit to the PDFs from all patches at +50 and −50 mV; the discrepancies between model and experimental PDFs in the other two patches were smaller than those shown in Fig. 8. Best values for the parameters are summarized in Table 1. For comparison, the parameters obtained by using a 50% threshold crossing analysis are

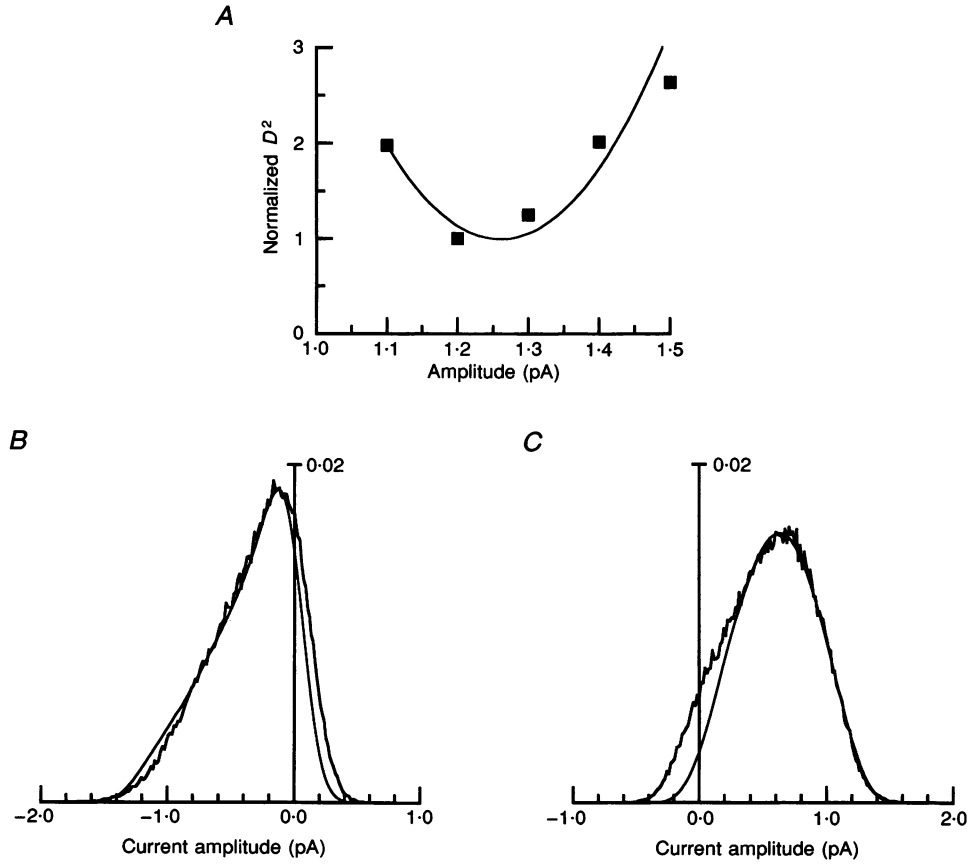

Figure 8. Fitting of a two-state model by computer simulations of channel activity

Results from patch 3 in 200 μM cGMP, with the ordinate scale for *B* and *C* being probability density per bin. *A*, determination of $\hat{\imath}$. The parameter $\hat{\imath}$ was varied between 1·1 and 1·5 pA, and the best-fitting simulation PDF was found at each amplitude. The continuous line shows the quadratic fit to the experimental results. The minimum occurred at 1·26 pA. *B*, amplitude PDF at −50 mV. The smooth continuous line shows a simulation fit of the two-state model to the PDF with $\beta = 0{\cdot}88 \times 10^4\ s^{-1}$, $\alpha = 2{\cdot}06 \times 10^4\ s^{-1}$ and $\hat{\imath} = -1{\cdot}26$ pA. *C*, amplitude PDF constructed from recordings obtained in 200 μM cGMP at +50 mV. The smooth continuous line shows a simulation fit of the two-state model to the PDF with $\beta = 2{\cdot}49 \times 10^4\ s^{-1}$, $\alpha = 2{\cdot}44 \times 10^4\ s^{-1}$ and $\hat{\imath} = 1{\cdot}26$ pA.

also shown. It is clear that the threshold analysis severely underestimated β and α. The threshold method also suggested that both parameters were voltage sensitive, while the simulation method indicated that only the opening rate constant β had significant voltage sensitivity (see below).

Voltage dependence of open–closed equilibrium of activated channels

Experimental PDFs at positive and negative voltages (e.g. Fig. 8*B* and *C*) were not symmetrical about 0 pA, indicating that the open–closed equilibrium of the active state was voltage sensitive. Fitting the experimental PDFs with simulations showed that the voltage dependence of channel activation could be explained by assuming that depolarization increased the rate constant β for channel opening, with little effect on α. This is different from the conclusion of Karpen *et al.* (1988*a*, *b*), who suggested that depolarization mainly reduced α on the basis of an analysis of macroscopic current relaxations after voltage jumps. The method employed here had a wider bandwidth than the previous experiments and did not require corrections for ion accumulation effects. Indeed the values for β and α estimated here are larger than those in the previous study.

Since values for β were available at two voltages, the voltage dependence of the rate constant could be obtained from the equation:

$$\beta = \beta_0 e^{(-zFV_m/RT)}, \quad (4)$$

where β_0 is the value of β at 0 mV, z is the equivalent number of electronic charges (e^+) that move across the membrane electric field during channel activation and V_m is the membrane potential. F and R are the usual physical constants and T is the absolute temperature. By plotting ln (β) *versus* V_m using the average of values for patches 2 and 3 (see Table 1), we obtained β_0 and z from the zero intercept and slope, respectively, of the line connecting the two data points. The values were: $\beta_0 = 15100\ s^{-1}$ and $z = 0{\cdot}23\ e^+$.

As shown in the Methods section (Fig. 1), the quality of the PDF fits was critically dependent on the ratio, β/α, of the two assumed rate constants. If we suppose that this ratio is well defined at both potentials, then the ratio β_{+50}/β_{-50} is a fixed multiple of $\alpha_{+50}/\alpha_{-50}$. Using the values for patches 2 and 3 from Table 1, $\beta_{+50}/\beta_{-50} = 2{\cdot}53\ \alpha_{+50}/\alpha_{-50}$. Because the magnitude of the rate constants was less well defined by the fits, there is some uncertainty as to how the voltage

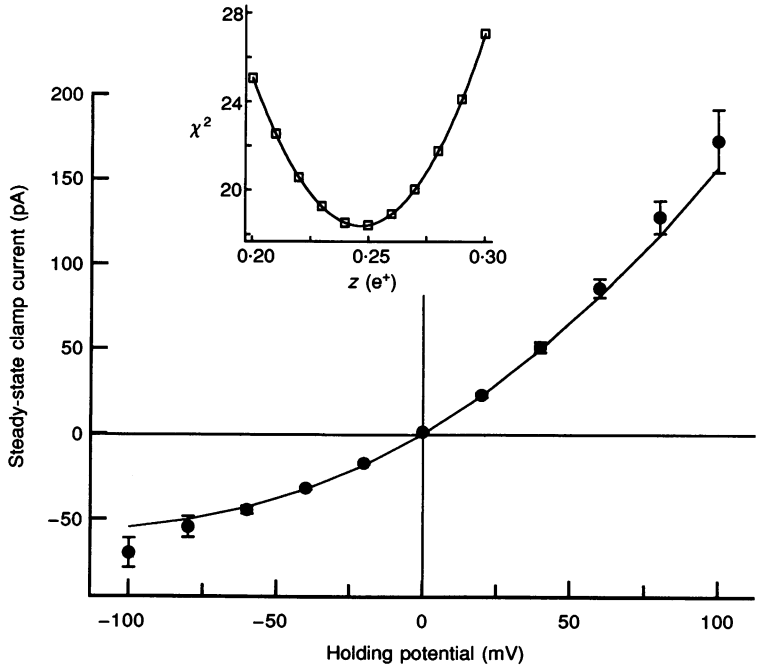

Figure 9. Voltage sensitivity of β

The filled symbols show the steady-state net 200 μM cGMP-activated membrane current (I_m) recorded during voltage steps over a range of membrane potentials. Each point represents the mean value from 5 patches. The continuous line was obtained from the fit of the equation:

$$I_m = GP_o(V_m - V_{rev}),$$

where P_o was obtained from eqn (5), $V_{rev} = 0$ mV and G is an arbitrary scaling factor. The inset shows the variation in the χ^2 value of the fit as the parameter z is varied. The minimum occurs at a value of 0·25, very close to the value obtained from the amplitude PDF analysis.

dependence of the transition is distributed between the two rate constants. If we conservatively allow the magnitude of α_{-50} to vary by 15%, this would correspond to a voltage dependence equivalent to $z = 0{\cdot}04e^+$ for α and to $z = 0{\cdot}19e^+$ for β. Thus, allowing for reasonable fitting errors, it seems that at least 80% of the voltage dependence resides with the opening rate constant β.

For the two-state model, the probability that the channel is open can be calculated from the equation:

$$P_o = \frac{\beta(V_m)}{\beta(V_m) + \alpha}. \quad (5)$$

Using the values of β_0 and z calculated above, eqn (5) was used to predict the form of the steady-state macroscopic current–voltage relation between +100 and −100 mV, as illustrated in Fig. 9. For the calculations the possible voltage dependence in the chord conductance of the open channel (Fig. 3*B*) was ignored. The agreement between theory and experimental results seems reasonable except at large negative voltages, where the experimental current was larger than the theoretical. There was also a suggestion that the measured outward currents increased more rapidly at positive potentials than the calculated currents.

We tested whether a different value for z would result from fitting only the steady-state current–voltage relation, again assuming a constant chord conductance for the open channel. For this test, z was varied between 0·20 and 0·30, and at each value of z, eqn (2) was evaluated with I_i as the measured steady-state values with standard deviations, σ_i, shown by the symbols with error bars in Fig. 9. The resulting χ^2 values are plotted against z in the inset of Fig. 9. The minimum on the χ^2 plot produced a value of $z = 0{\cdot}25 \pm 0{\cdot}04e^+$ (90% confidence interval). The good agreement between the values for z obtained from the single channel PDFs and the macroscopic current–voltage relations is encouraging, and suggests that the two-state model described here provides a picture of the channel mechanics that is at least internally consistent.

DISCUSSION

Single channel conductance

The results described here confirm previous reports of a 'subconductance state' of the cyclic GMP-activated channel (Haynes *et al.* 1986; Zimmerman & Baylor, 1986; Tanaka, Furman, Cobbs & Mueller, 1987). In two other studies of the salamander rod channel, the smaller current level was not observed. Matthews & Watanabe (1988) did not detect the smaller current level in single channel patches from the inner segment, but they recorded only at negative potentials, where the small currents are not obvious. Torre *et al.* (1992) also failed to detect the smaller currents in

Table 1. Comparison of rate constants derived from analysis of channel activity in 50 μM (patch 2) and 200 μM cGMP at +50 and −50 mV

	Patch	β		α		P_o	î (pA)
Analysis (+50 mV)							
PDF	1	29800	(34)	17200	(58)	0·63	1·26
	2	22600	(44)	18200	(55)	0·55	1·28
	3	24900	(40)	24400	(41)	0·51	1·26
Mean		25800	(39)	19900	(51)	0·56	1·27
50% threshold crossing	1	7870	(130)	2630	(380)	0·75	
	2	4440	(225)	1520	(660)	0·74	
	3	5260	(190)	3310	(300)	0·61	
Mean		5860	(180)	2490	(402)	0·70	
Analysis (−50 mV)							
PDF	2	10500	(95)	24200	(41)	0·30	−1·28
	3	8800	(114)	20600	(49)	0·30	−1·26
Mean		9650	(104)	22400	(45)	0·30	
50% threshold crossing	2	1740	(524)	4380	(228)	0·28	
	3	1910	(575)	6370	(157)	0·23	
Mean		1830	(550)	5380	(193)	0·25	

The opening rate constant, β (s^{-1}), the closing rate constant, α (s^{-1}) and the current amplitude (î), were estimated from computer simulation as described in the text. P_o is the open probability where $P_o = \beta/(\alpha + \beta)$. The predicted mean dwell times (τ, μs) in the closed state ($1/\beta$) and the open state ($1/\alpha$) are shown in parentheses next to the rate constants. Although saturation of the response was clearly seen for patch 2, an increase in the baseline noise level later during the recording made it necessary to analyse the 50 μM data.

multichannel patches which were recorded at both positive and negative potentials. Multiple conductance states are observed when the bovine channel is inserted into planar lipid bilayers (Hanke *et al.* 1988; Bennett & Clerc, 1989; Ildefonse & Bennett, 1991), but these channels appear to have slower activation kinetics and a lower sensitivity to cGMP than the channel of salamander rods.

The value of 25 pS estimated here for the open-state conductance of the channel at +50 mV is in good agreement with two previous values for the amphibian rod channel (Haynes *et al.* 1986, ~25 pS; Zimmerman & Baylor 1986, ~24 pS). Torre and his colleagues (Torre *et al.* 1992; Sesti *et al.* 1994), however, estimated from noise analysis that the open channel conductance of the channel in outer segment patches was greater than 55–60 pS. In about 10% of the patches excised from the inner segment, single channels with a well-resolved level of 28 pS were observed. These latter channels did not flicker, unlike those described here. We suggest that both types of channel, those with and without flicker, may have similar open-state conductances. Recent evidence suggests that flicker occurs in hetero-multimeric channels containing a newly discovered subunit (Chen *et al.* 1993).

The instantaneous I–V relations obtained at early times from patches with multiple channels (Fig. 3*B*, this paper and Fig. 6*A*, Zimmerman & Baylor, 1992) showed slight outward rectification, and the rectification was somewhat more pronounced in the steady state. Zimmerman & Baylor (1992) suggested that the rectification at early times (50 μs) might depend mainly on the voltage dependence of ion permeation through the open channel, but the present analysis suggests that the voltage dependence of gating must make some contribution, even at these early times, since the gating time constant is predicted to drop below 25 μs at voltages positive to +20 mV.

Magnitude and voltage dependence of rate constants for channel gating

At +50 mV the rate constants α and β in the two-state model were estimated as $2{\cdot}0 \times 10^4$ s^{-1} and $2{\cdot}6 \times 10^4$ s^{-1}, respectively. The relaxation time constant, τ, calculated as $\tau = 1/(\alpha + \beta)$, is about 22 μs. The fluctuations of the system should have a Lorentzian power spectrum with cut-off frequency $1/2\pi\tau = 7{\cdot}3$ kHz. Sesti *et al.* (1994) have reported that multichannel patches from rod outer segments indeed exhibit noise that rolls off at frequencies higher than 5 kHz. Using the 50% threshold method, Haynes & Yau (1990) and Matthews & Watanabe (1987, 1988) have obtained values for $1/\beta$ and $1/\alpha$ in the range 0·1–0·5 ms. Similar values were obtained here by the use of the threshold method (see Table 1), yet the simulations indicate that gating is considerably faster, and simulations with the slower rate constants could not reconstruct the experimental PDFs.

In the two-state model assumed to apply at saturating cGMP, the probability that the channel will be open (P_o) is $P_o = \beta/(\alpha + \beta)$. We estimate that at −70 mV, $P_o = 0{\cdot}27$. This is very close to the value of 0·30 at −70 mV obtained by Matthews & Watanabe (1988) using threshold analysis. At +50 mV we found that $P_o = 0{\cdot}56$, which is less than the value of 0·86 inferred previously by Karpen *et al.* (1988*a*).

The single channel recordings confirm steady-state macroscopic current measurements, indicating that channel activation by cGMP is voltage dependent (Matthews, 1987; Karpen *et al.* 1988*a*; Furman & Tanaka, 1989; Tanaka, Eccleston & Furman, 1989; Menini, 1990; Ildefonse & Bennett, 1991). As the membrane potential was made more positive, P_o increased and analysis of the PDFs indicated that this resulted from the voltage dependence of β. This explanation differs from that of Karpen *et al.* (1988*b*), who attributed the voltage dependence of channel activity to that of the closing rate constant, α. The magnitude of the voltage dependence found here, with an equivalent gating charge $z = 0{\cdot}23e^+$ is similar to that found in previous studies ($z = 0{\cdot}3e^+$, Ildefonse & Bennett, 1991; $z = 0{\cdot}17e^+$, Tanaka *et al.* 1989; $z = 0{\cdot}20e^+$, Karpen *et al.* 1988*a*).

A model for channel activation

The data presented above suggest a model of channel activation represented by the scheme:

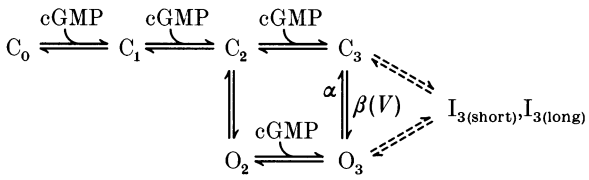

where C_i are the closed-states, O_i are the open-states and the subscript i indicates the number of agonist molecules bound. It must be emphasized that this is a minimal scheme; since the channel may be tetrameric it seems likely that more than three cGMP binding sites contribute to channel activation. Similar schemes have been proposed by others (Karpen *et al.* 1988*a*; Haynes & Yau, 1990; Ildefonse & Bennett, 1991). In this section we summarize the evidence that supports this model.

We shall ignore for the moment the extra closed states, I_3. The four closed states, differing only in the number of agonist molecules bound, are required to account for the Hill coefficient of 2–3 observed here and in a number of other studies (Haynes *et al.* 1986; Tanaka *et al.* 1987; Karpen *et al.* 1988*a*; Matthews & Watanabe, 1988; Haynes & Yau, 1990; Chen *et al.* 1993). Analysis of amplitude PDFs indicates that the small activated state occurs more frequently at subsaturating concentrations of cGMP, suggesting that the substate is reached from a partially liganded channel state. Inspection of the records in Fig. 6*A* suggests that the channel can open to the substate and close again without passing through the fully open state. Further, the substate can apparently be reached from the fully open state. These observations suggest the connections

of O_2 with O_3 and C_2, allowing us to assign O_2 to the small activated state, 4 pS, and O_3 to the full conductance state, 25 pS. It also appears that the channel can open and close without entering the substate, supporting the connection of C_3 with C_2 and O_3. Although this scheme for connecting the states seems consistent with the results to date, it should be regarded as tentative rather than proved. Goulding *et al.* (1992) presented evidence that a substate in cyclic nucleotide-activated channels of olfactory neurons is due to block by external protons, and we cannot rule out the possibility that block by protons produces the substate in the rod channel. Quantitative analysis of the amplitude PDFs at saturating cGMP indicated that the entire voltage dependence of the channel gating resides in the $C_3 \rightarrow O_3$ transition, with the rate constant $\beta(V)$ dependent on membrane potential. Earlier work (Karpen *et al.* 1988*a*) suggests that the voltage dependence of channel activation at subsaturating cGMP may result from the voltage dependence of the $O_3 \rightarrow C_3$ transition.

We have included two extra fully liganded closed channel states, $I_{3(short)}$ and $I_{3(long)}$, to account for the short and long gaps observed in recordings at saturating cGMP. The dashed lines indicate uncertainty as to which channel state(s) $I_{3(short)}$ and $I_{3(long)}$ are connected. At saturating concentrations of cGMP, and assuming diffusion limited binding rates, the reaction scheme for the channel can be reduced to two states (C_3 and O_3), each having the maximum number of cGMP molecules bound. If the rate constants connecting these two states are large, the current will display the flicker that dominates the records shown in Fig. 2. In agreement with Torre *et al.* (1992), such flicker does not appear to be the result of block by divalent cations, as free divalent ion concentrations were very low in solutions containing 100 μM EDTA .

In all three patches analysed, however, the form of the amplitude PDFs was not entirely consistent with a simple two-state model; the channel spent more time closed than expected, evident as excess density at low amplitudes in the PDFs. It is important to note that this excess density was clearly present at saturating concentrations of cGMP and therefore cannot be attributed to the occupation of the small activated state. The longest of the events contributing to this extra closed time, a few tens of milliseconds in duration, can be observed directly in the single channel records. Since we excluded long gaps from the analysis (designated $I_{3(long)}$ in the model), we propose that there is at least one other fully liganded closed state (designated $I_{3(short)}$ in the model).

We can give an upper limit for the total duration of the short gaps from the 200 μM cGMP, +50 mV PDFs, if one accepts that the excess density in the PDFs at 0 pA, is due, at least in part, to the presence of the short gaps. For the three patches at +50 mV, the excess densities unaccounted for by the two-state model were 2, 12 and 9% respectively. The events observable in Figs 2*A* and 4 indicate that the duration of the short gaps is in the order of 10 ms. Therefore, we would expect roughly one to ten short gaps per second. The frequency of the $I_{3(short)}$ events was too high and the duration far too short for them to be considered long gaps which lasted hundreds of milliseconds to several seconds and which occurred with a frequency roughly two orders of magnitude lower.

Proton block, flicker and the subconductance state

A possible physical mechanism for the rapid flicker of the single channel current is suggested by previous results demonstrating that block of olfactory cAMP channels (Goulding *et al.* 1992), and L-type calcium channels (Prod'hom, Pietrobon & Hess, 1987) by protons from the external solution, can produce a subconductance state. As binding and unbinding occur very rapidly, the current through the channel flickers between two levels. Could a similar proton block underlie the subconductance state and rapid flicker in the single channel currents reported here? We have no direct evidence for this, but three points are worth noting. Firstly, if block by protons produces the subconductance state in the cGMP-activated channel, the concentration dependence of the subconductance state implies that proton block was more effective in the partially liganded channel. In contrast, Goulding *et al.* (1992) found that the occurrence of the subconductance state in the olfactory channel was independent of nucleotide concentration. Furthermore, a change in the degree of block with ligand concentration should produce concentration-dependent changes in the shape and position of the major peak of the amplitude distributions in Fig. 6*C*, yet this was not observed. Secondly, in both previous studies, the proton block was independent of membrane potential at negative voltage. If proton block underlies the rapid gating transitions observed here, the block would need to be voltage dependent. Finally, the conductance of the olfactory cAMP channels is considerably larger than that described here, suggesting fundamental differences in the two permeation pathways.

Bennett, N. & Clerc, A. (1989). Activation of cGMP phosphodiesterase in retinal rods: Mechanism of interaction with the GTP-binding protein (transducin). *Biochemistry* **28**, 7418–7424.

Chen, T.-Y., Peng, Y.-W., Dhallan, R. S., Ahmed, B., Reed, R. R. & Yau, K.-W. (1993). A new subunit of the cyclic nucleotide-gated cation channel in retinal toads. *Nature* **362**, 764–767.

Fesenko, E. E., Kolesnikov, S. S. & Lyubarsky, A. L. (1985). Induction by cyclic GMP of cationic conductance in plasma membrane of retinal rod outer segments. *Nature* **313**, 310–313.

FitzHugh, R. (1983). Statistical properties of the asymmetric random telegraph signal, with applications to single channel analysis. *Mathematical Bioscience* **64**, 75–89.

FURMAN, R. E. & TANAKA, J. C. (1989). Photoreceptor channel activation: Interaction between cAMP and cGMP. *Biochemistry* **28**, 2785–2788.

GOULDING, E. H., NGAI, J., KRAMER, R. H., COLICOS, S., AXEL, R., SIEGELBAUM, S. A. & CHESS, A. (1992). Molecular cloning and single-channel properties of the cyclic nucleotide-gated channel from catfish olfactory neurons. *Neuron* **8**, 45–58.

HANKE, W., COOK, N. J. & KAUPP, U. B. (1988). cGMP-dependent channel protein from photoreceptor membranes: Single channel activity of the purified and reconstituted protein. *Proceedings of the National Academy of Sciences of the USA* **85**, 94–98.

HAYNES, L. W., KAY, A. R. & YAU, K.-W. (1986). Single cyclic GMP-activated channel activity in excised patches of rod outer segment membrane. *Nature* **321**, 66–70.

HAYNES, L. W. & YAU, K. W. (1990). Single-channel measurement from the cyclic CMP-activated conductance of catfish retinal cones. *Journal of Physiology* **429**, 451–481.

ILDEFONSE, M. & BENNETT, N. (1991). Single-channel study of the cGMP-dependent conductance of retinal rods from incorporation of native channels into planar lipid bilayers. *Journal of Membrane Biology* **123**, 133–147.

KARPEN, J. W., ZIMMERMAN, A. L., STRYER, L. & BAYLOR, D. A. (1988*a*). Gating kinetics of the cyclic-GMP-activated channel of retinal rods: Flash photolysis and voltage-jump studies. *Proceedings of the National Academy of Sciences of the USA* **85**, 1287–1291.

KARPEN, J. W., ZIMMERMAN, A. L., STRYER, L. & BAYLOR, D. A. (1988*b*). Molecular mechanics of the cyclic-GMP-activated channel of retinal rods. *Cold Spring Harbour Symposia on Quantitative Biology* **LIII**, 325–332.

KAUPP, U. B., NIIDOME, T., TANABE, T., TERADA, S., BÖNIGK, W., STÜHMER, W., COOK, N. J., KANGAWA, K., MATSUO, H., HIROSE, T., MIYATA, T. & NUMA, S. (1989). Primary structure and functional expression from complementary DNA of the rod photoreceptor cyclic GMP-gated channel. *Nature* **342**, 762–766.

MATTHEWS, G. (1987). Single-channel recordings demonstrate that cGMP opens the light-sensitive ion channel of the rod photoreceptor. *Proceedings of the National Academy of Sciences of the USA* **84**, 299–302.

MATTHEWS, G. & WATANABE, S. (1987). Properties of ion channels closed by light and opened by guanosine 3′,5′-cyclic monophosphate in toad retinal rods. *Journal of Physiology* **389**, 691–715.

MATTHEWS, G. & WATANABE, S. (1988). Activation of single ion channels from toad retinal rod inner segments by cyclic GMP: concentration dependence. *Journal of Physiology* **403**, 389–405.

MENINI, A. (1990). Currents carried by monovalent cations through cyclic GMP-activated channels in excised patches from salamander rods. *Journal of Physiology* **424**, 167–185.

PROD'HOM, B., PIETROBON, D. & HESS, P. (1987). Direct measurement of proton transfer rates to a group controlling the dihydropyridine-sensitive Ca^{2+} channel. *Nature* **329**, 243–246.

SESTI, F., STRAFORINI, M., LAMB, T. D. & TORRE, V. (1994). Gating, selectivity and blockage of single channels activated by cyclic GMP in retinal rods of the tiger salamander. *Journal of Physiology* **474**, 203–222.

TANAKA, J. C., ECCLESTON, J. F. & FURMAN, R. E. (1989). Photoreceptor channel activation by nucleotide derivatives. *Biochemistry* **28**, 2776–2784.

TANAKA, J. C., FURMAN, R. E., COBBS, W. H. & MUELLER, P. (1987). Incorporation of retinal rod cGMP-dependent conductance into planar bilayers. *Proceedings of the National Academy of Sciences of the USA* **84**, 724–728.

TORRE, V., STRAFORINI, M., SESTI, F. & LAMB, T. D. (1992). Differential channel-gating properties of two classes of cyclic GMP-activated channel in vertebrate photoreceptors. *Proceedings of the Royal Society* B **250**, 209–215.

YELLEN, G. (1984). Ionic permeation and blockade in Ca^{2+}-activated K^+ channels of bovine chromaffin cells. *Journal of General Physiology* **84**, 157–186.

ZIMMERMAN, A. L. & BAYLOR, D. A. (1986). Cyclic GMP-sensitive conductance of retinal rods consists of aqueous pores. *Nature* **321**, 70–72.

ZIMMERMAN, A. L. & BAYLOR, D. A. (1992). Cation interactions within the cyclic GMP-activated channel of retinal rods from the tiger salamander. *Journal of Physiology* **449**, 759–783.

Acknowledgements

We thank Dr William Zagotta for helpful comments on the manuscript. Supported by grant EY01543 from the National Eye Institute, US Public Health Service.

Received 13 June 1994; accepted 5 September 1994.